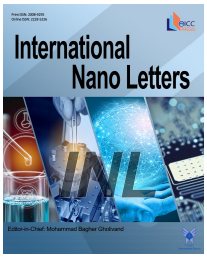

Volume 15, Issue 1, 152502 (1-14)

International Nano Letters (INL)

https://doi.org/10.57647/inl.2025.1401.02

PMMA/TiO_2 Nanocomposite Derived Selective Surface Coatings for Improved Optical Properties with Cold Plasma Assisted

Rasheed N. Abed[1*], Hassan Hashim[2], Muataz Ali[3], Roaa T. Abdulla[4], Ali B. M. Ali[5], Mohammed Al-Baidhani[4], Kadhim A. Aadim[6], Abdulrahman H. Shaker[6], Khalid Zainulabdeen[3], Ahmed A. Alamiery[7], Muna S. Bufaroosha[8*], Emad Yousif[3]

[1]*Department of Mechanical Engineering, College of Engineering, Al-Nahrain University, P.O. Box: 64040, Jadriyah, Baghdad, Iraq.*
[2]*Department of Medical Physics, College of Science, Al-Nahrain University, P.O. Box: 64021, Jadriyah, Baghdad, Iraq.*
[3]*Department of Chemistry, College of Science, Al-Nahrain University, P.O. Box: 64021, Jadriyah, Baghdad, Iraq.*
[4]*Department of Physics, College of Science, Al-Nahrain University, P.O. Box: 64021, Jadriyah, Baghdad, Iraq.*
[5]*Air Conditioning Engineering, Faculty of Engineering, Warith Al-Anbiyaa University, Karbala 56001, Iraq.*
[6]*Department of Physics, College of Science, University of Baghdad, Baghdad, Iraq.*
[7]*Al-Ayen Scientific Research Center, Al-Ayen Iraqi University, AUIQ, Al-Nasiriyah, P.O. Box: 64004, Thi Qar, Iraq.*
[8]*Department of Chemistry, College of Science, United Arab Emirates University, Al-Ain, United Arab Emirates.*

[*]**Corresponding author:** rasheed.n.abed@nahrainuniv.edu.iq, muna.bufaroosha@uaeu.ac.ae

Original Research

Received:
8 Januanry 2025
Revised:
18 February 2025
Accepted:
24 March 2025
Published online:
31 March 2025

Abstract:

Progressive evolution of nanostructured coatings with costume-made structural and optical properties is of major interest for different high-tech applications. This work targeted the incorporation of titanium dioxide (TiO_2) nanoparticles to poly(methyl methacrylate) (PMMA) nanocomposite films across three concentrations (1%, 2%, and 3%) using the casting method. These films were later treated with cold dielectric barrier discharge (DBD) plasma to refine their structure and optical properties. Investigations were systematically studied through the work including the extinction coefficient, absorption coefficient, dielectric constant (real and imaginary), energy gap, Urbach energy, and refractive index. A significant increase resulted in the real dielectric constant, refractive index, and absorption coefficient, on the other hand, a decrease due to strong absorption was noted in the imaginary dielectric constant and extinction factor. Direct and indirect energy gap ranged from 4.7 to 4.5 eV, and 3.4 to 3.25 eV, respectively. Urbach energy data elevated from 366 to 395 meV, which suggests improved charge carrier transport attributed to structural modifications achieved by plasma induction. Also, cold DBD plasma treatment efficiently increased the roughness of the surface, and as a result, improved the film's optical absorption abilities. These findings were confirmed using structural analysis, X-ray diffraction (XRD) showed a mixture of semi-crystalline and amorphous phases. SEM examined revealed a uniform TiO_2 distribution across the PMMA accompanied by gaining a roughened morphology. AFM analysis also showed a boost in surface roughness from 0.828 to 3.04 nm after incorporating TiO_2 and applying plasma treatment. These results propose that PMMA/TiO_2 nanocomposite films showed encouraging potential for applications in fiber optics, optical sensors, photocatalysis, and light-emitting diodes (LEDs).

Keywords: Cold DBD plasma; Titanium oxide (TiO_2); Poly(methyl methacrylate) (PMMA); Nanocomposite films (PMMA/TiO_2); Optical conductivity; Urbach energy

Cite this article: Abed R.N., Hashim H., Ali M., Abdulla T., Ali A.B.M., Al-Baidhani M., Aadim K.A., Shaker A.H., Zainulabdeen K., Alamiery A.A., Bufaroosha M.S., Yousif E. PMMA/TiO_2 Nanocomposite Derived Selective Surface Coatings for Improved Optical Properties with Cold Plasma Assisted. *Int. Nano Lett.* **15**(1), 152502 (2025).

1. Introduction

Titanium dioxide (TiO_2) as a compound has been widely used in different applications because of its remarkable chemical stability, photocatalytic ability, and optical characteristics. It performs a significant role in environmental applications, such as hazardous waste management [1], purification [2], sterilization [3], photocatalysis [4], self-cleaning surfaces [5], dye-sensitized solar cells [6, 7], and hydrogen generation [8]. TiO_2 nanoparticles gathered extensive research consideration because of their environmental-friendly properties, effective catalysis ability under UV light, and remarkable resistance to heat exposure [9–11]. Also, the photocatalytic role of TiO_2 on thin-film surfaces has been consistently used to assist in oxidation-reduction mechanisms, UV light stimulates electron-hole pairs generation on surface, TiO_2 interacts with particles adsorbed on the surface, enabling the catalytic reactions [12–14]. Additionally, because of its structural and chemical robustness, TiO_2 acts as an enhancement additive in polymer matrices, improving polymer structure and assisting in the improvement of optimized nanocomposite films [15].

Despite their extensive applications, polymers are often recognized for their weak mechanical strength and thermal conductivity compared to metals and ceramics. Nevertheless, their pros like lightweight and cost make them appealing to many medical and engineering applications. The characteristics of polymeric materials might be markedly enhanced by doping appropriate nanofillers, enabling the formation of nanocomposite materials with enhanced properties [16]. Incorporating nanoparticles into polymer matrices, develops a unique nanocomposite with improved electrical and optical properties, enabling promising prospects in photoelectronic and photocatalytic applications [17]. Nanocomposite films are particularly beneficial due to their long-lasting durability, wide availability, relative flexibility, comparatively lightweight, and cost-effectiveness [18–20].

Poly(methyl methacrylate) (PMMA) is commonly acknowledged across polymers for its non-crystalline structure, linear polymer chains, cost feasibility, transparent nature, impact durability and lightweight property. Its erosion resistance and durability make it a dependable substitute for inorganic glass in many applications [21]. In addition, PMMA exhibits significant stability against thermal variations and acidic media, contributing to its inertness in aqueous media, and preventing hydrolysis efficiently [22]. Although the use of pure PMMA in the purification of water is relatively limited, nanocomposites of PMMA/TiO_2 have demonstrated a promising alternative as membrane materials attributed to their relatively large surface area, improved stability, enhanced electrical conductivity, and surface reactivity [23]. Furthermore, incorporating PMMA with nanoparticles such as copper oxide (CuO), chromium oxide (Cr_2O_3), and cobalt oxide (Co_3O_4) has shown a significant enhancement to its optoelectronic and optical properties [24].

While prior research's focus was on enhancing the existing PMMA structures through the integration of nanomaterials, this work employs cold dielectric barrier discharge (DBD) plasma treatment to modify the surface characteristics of PMMA/TiO_2 nanocomposite films.

This approach proved to be able to facilitate surface modification and form of different functional groups, enhancing biocompatibility, while conserving the polymer's characteristics [25, 26]. Treatment with atmospheric plasma initiates oxidative changes, improving adhesion and interfacial shear strength inside polymer chains [27]. In addition, the plasma technique has been considered a successful approach to improve the dispersion of nanoparticles within polymer structure, thereby enabling consistent distribution and improved molecular interactions [28, 29].

In this regard, this work intends to design a novel surface coating by doping TiO_2 nanoparticles into PMMA thin films at different concentration percentages (1%, 2%, and 3%). The surface texture and optical characteristics of these doped films were methodically experimented to evaluate the effect of TiO_2 doping and the later plasma treatment. X-ray diffraction (XRD) tests verified a semi-crystalline and amorphous structure, while, scanning electron microscopy (SEM) showed a homogeneous TiO_2 layer and improved surface texture. DBD plasma system exposure significantly enhanced absorption abilities, improving charge carrier mobility through conduction and valence bands. Results proved the potential ability of PMMA/TiO_2 nanocomposite films for utilization in fiber optics, optical sensors, photocatalysis, and LED technologies.

2. Experimental work

2.1 Material and methods

PetKim Petrokimya in Istanbul, Turkey, provided the blank poly(methyl methacrylate) (PMMA) material, while China/Hunan/Changsha Easchem company supplied the titanium oxide (TiO_2) nanoparticles (purity of 99.98% and particle size of 18 nm). The film's structure was ascertained using an XRD apparatus (X-Pert Pro, Cu-Kα radiation ($\lambda = 1.540$ Å), Bragg's angle (2θ) with a tube at 30 kV, (see Supplementary Fig. 1 (a)). Nanocomposite film diffusive reflectance (DH-S-BAL-2048, Avantes) was measured in a 0.6-step range between 238 and 1238 nm, which is used to inspect the films of PMMA/TiO_2 (see Supplementary Fig. 1 (b)). Atomic force microscopy (AFM) (AA2000, Angstrom, under atmospheric conditions) was utilized to illustrate the surface roughness of PMMA/TiO_2 thin films, (see Supplementary Fig. 2). The digital micrometer (PosiTector 6000) device has been used to measure the thickness of the samples, while this thickness was used in calculations.

Cold plasma device, that is run at a current AC with a voltage of up to 25 kV and a cut-off frequency of up to 150 kHz. In the laboratory assembly and customization were achieved for a hand-made dielectric barrier discharge (DBD) cold plasma device, as illustrated in Supplementary Fig. 3 (a). In this configuration, the cold DBD plasma is produced when the samples are placed between two electrodes, the gab maintained between the plasma electrode and the sample where 2 mm, as shown in Supplementary Fig. 3 (b).

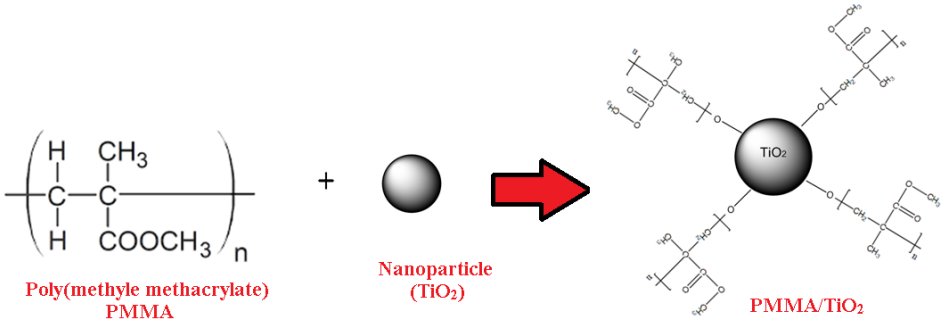

Scheme 1. PMMA/TiO_2 nanocomposite displays TiO_2 dangled between PMMA matrix.

2.2 Synthesis the nanocomposite thin film

2.2.1 Fabrication of PMMA/TiO_2 nanocomposite films

In the lab, 25 mL of chloroform ($CHCl_3$) was mixed with 6 g of PMMA for 20 min at 30 °C, the dissolved polymer was refluxed for 2 hrs. with continuous stirring. Later, 18 nm nanoparticles of TiO_2 were added to the precursor solution in percentages of 1, 2, and 3 wt.%. Sonication was applied to the mixture in an ultrasonic device for two hours. Resulted solution was molded, forming PMMA/TiO_2 nanocomposite films with the nanoparticles dangled between the PMMA lattice as a doped filler, where the samples had a thickness of 40 µm. The concentrations quantities of the PMMA/TiO_2 nanocomposite films are shown in the Supplementary Table 1.

The nanocomposite films were allowed to dry at 30 °C for 72 hrs. Additionally, an extra 2 hrs. of drying in a vacuum was conducted to eliminate any remaining solvents before taking measurements. The structure of the PMMA/TiO_2 nanocomposite film samples is illustrated in Scheme 1, where the TiO_2 nanoparticles are embedded within the PMMA matrix.

2.2.2 Synthesis of PMMA/TiO_2 nanocomposite films under cold plasma exposure

The PMMA/TiO_2 nanocomposite films were exposed to the cold DBD plasma in ambient air to optimize the nanocomposite structure in order to improve its optical properties. The electron temperature values were calculated using the Boltzmann equation (see equation (1)). The ratio method used in Optical Emission Spectroscopy (OES) is well established to be used techniques for this purpose [30–32]:

$$\ln\left[\frac{\lambda_{ji}I_{ji}}{hcA_i g_j}\right] = \frac{1}{k_B T}(E_j) + \ln\left[\frac{N}{U(T)}\right] \quad (1)$$

where (I_{ji}) the relative emission line density between energy levels i and j, (g_j) the degeneracy or the upper level statistical weight emitted from the transition phase, (λ_{ji}) the wavelength (nm), (E_j) the excitation energy (eV) for level j, (A_i) the automatic transmission possibility of radiation from the level i to the lower level j, N is the density of the state population, and (k_B) the Boltzmann constant.

Thereby, Fig. 1 (A) shows the boltizman plot between $\ln[\frac{\lambda_{ji}I_{ji}}{hcA_i g_j}]$ against the excitation energy (E_j) and then find the temperature of electron (T_e).

Consequently, Fig. 1 (B) represents the plasma optical emission spectrum of the DBD plasma in air to find the data of the intensity, and with the NIST database to find the density of plasma electron, as shown in equation (2) [33]:

$$n_e = \left(\frac{\Delta\lambda_{\mathrm{FWHM}}}{2\omega_s}\right) N_r \quad (2)$$

where: $\Delta\lambda_{\mathrm{FWHM}}$ the full width half maximum (nm), (ω_s) the Stark broadening parameter can be obtained from standard tables, (N_r) the reference electron density.

The optical spectrum of DBD plasma was determined by the spectroscopy of optical emission (OES) technique, Fig. 1 (B) represents the intensity as a function of wavelength.

The other parameters such as plasma frequency (f_p) and

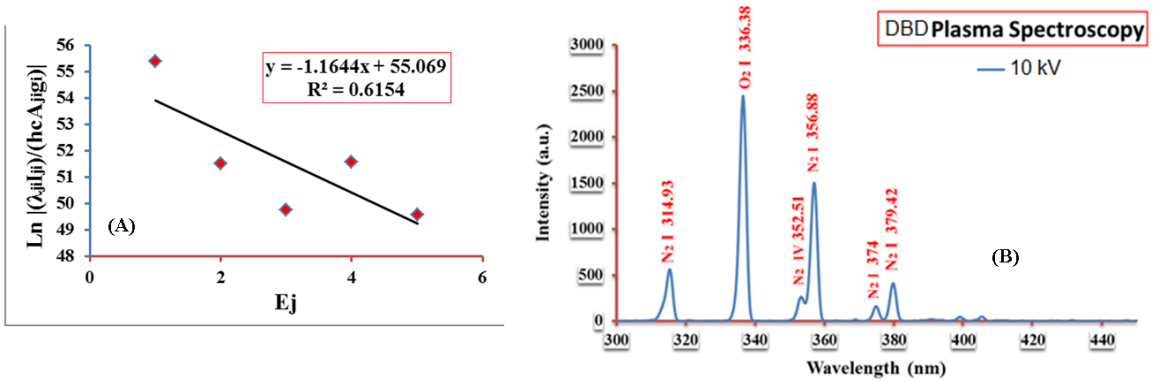

Figure 1. (A) Boltzmann plots for 10 kV applied voltage of DBD plasma system, (B) DBD plasma system Spectrum at AC applied voltage of 10 kV.

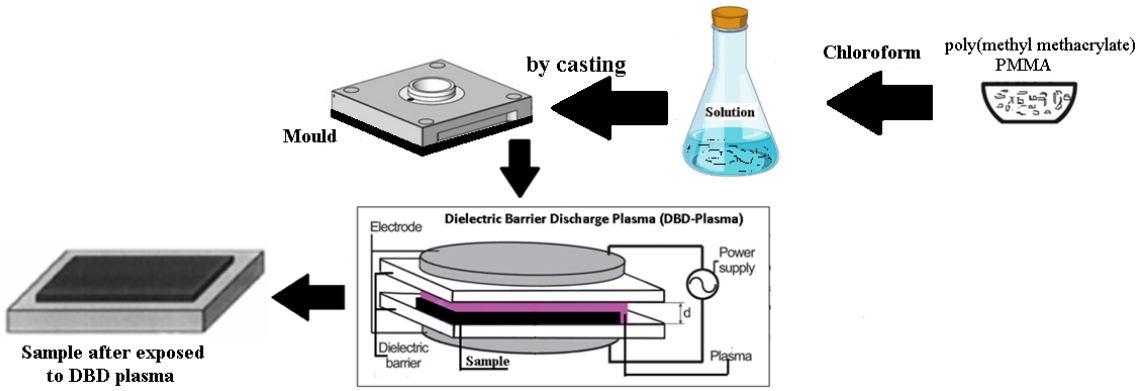

Figure 2. The PMMA/TiO_2 nanocomposite films when focused by DBD plasma system.

Debye length (λ_D) can be calculated from equation (3) [34]:

$$\begin{bmatrix} f_p = 9000\sqrt{n_e} \\ \\ \lambda_D = \frac{n_e e^2}{\varepsilon_0 m_e} \end{bmatrix} \quad (3)$$

where, (n_e) plasma electron density, (e) electron charge, (ε_0) free space permittivity, and (m_e) electron mass.

The results of Plasma parameters T_e, f_p, λ_D, $\Delta\lambda_{FWHM}$ and n_e for DBD plasma system were listed in Supplementary Table 2.

The PMMA/TiO_2 nanocomposite films were activated via dielectric barrier discharge (DBD) at atmospheric air conditions. The setup utilized a power source configured to function in AC modes, with voltages reaching a maximum of 25 kV and a cut-off frequency of up to 150 kHz. The DBD disks are linked to the anode and cathode terminals of the power supply, as depicted in Fig. 2. Blank and nanocomposite samples, fabricated with different TiO_2 concentrations (1%, 2%, and 3%) for PMMA doping, are placed between the electrodes with a 2 mm separation between the disks. An AC voltage of around 10 kV at a frequency of 50 Hz is applied, with each sample exposed for 30 seconds.

3. Results and discussion

3.1 XRD analysis

X-ray diffraction (XRD) spectra of PMMA thin films with different TiO_2 concentrations are shown in Fig. 3 (A) analysis shows low-intensity diffraction peaks related to PMMA/TiO_2 nanocomposites at doping percentages of 1%, 2%, and 3%. The intact PMMA film showed no visible peaks, implying its amorphous texture.

Regarding the PMMA nanocomposite incorporated with 1% TiO_2, three small diffraction peaks were detected at 2θ angles of 32°, 35°, and 37°. The 2% TiO_2-PMMA nanocomposite showed two minor peaks at 32° and 37°, while the 3% TiO_2-doped composite revealed three peaks at 32°, 35°, and 37°. TiO_2 existence in the PMMA nanocomposite is regarded as the doping of TiO_2 nanoparticles within the polymer structure. Also, the presence of minor peaks implies nanoparticles existing within the polymer chains, marking a structure that is principally amorphous alongside semi-crystalline properties.

Additionally, for films that have been treated with plasma, the amplitude of the diffraction peaks elevated as a result of TiO_2 doping and cold dielectric barrier discharge (DBD) plasma exposure, causing improved crystallinity of the samples [35, 36].

3.2 Absorption coefficient and reflectance of PMMA/TiO_2

Absorption coefficient (α) is critical in material characteristics because it depends on electrons movement within orbitals. When electrons within orbitals are impacted with specific wavelength spectra, a part of the light is absorbed, pushing electrons to an exciting state and easing their movement across energy levels. The absorption coefficient is calculated by applying the equation (4) [37, 38].

$$\alpha = 2.303 \times \frac{A}{t} \quad (4)$$

where: α; absorption coefficient (cm^{-1}), A absorbance value, and (t) coating thickness (cm).

Fig. 3 (B) and (C) shows the absorption coefficient and reflectance of raw PMMA and PMMA/TiO_2 nanocomposites films with various TiO_2 percentages (1, 2, and 3 wt.%). Fig. 3 (B) five spectra shows the absorption coefficient, and the data in Fig. 3 (C) displays the reflectance.

Absorption coefficient starts at the smaller wavelength values where the device starts, and goes up to a 120 cm^{-1}. This boosted absorption value is caused by the TiO_2 doping and the structural improvements effected by treatment with plasma, as shown in Fig. 3 (B). Also, Fig. 3 (C) shows a reflectance reduction after doping with TiO_2 and treatment with plasma. This might prove a variation in the polymer chain composition after nanoparticles addition and DBD plasma contact. As a result, the reflectance data changes down from 50% to 11%, while the absorbance data range from 83% and 89% [39].

3.3 Refractive index and extinction factor of PMMA/TiO_2

Refractive index (n) is related to electron polarization, which generates according to molecular rotation in the exact position influenced by an electric field. therefore, the refractive index (n) is calculated using equation (5) below

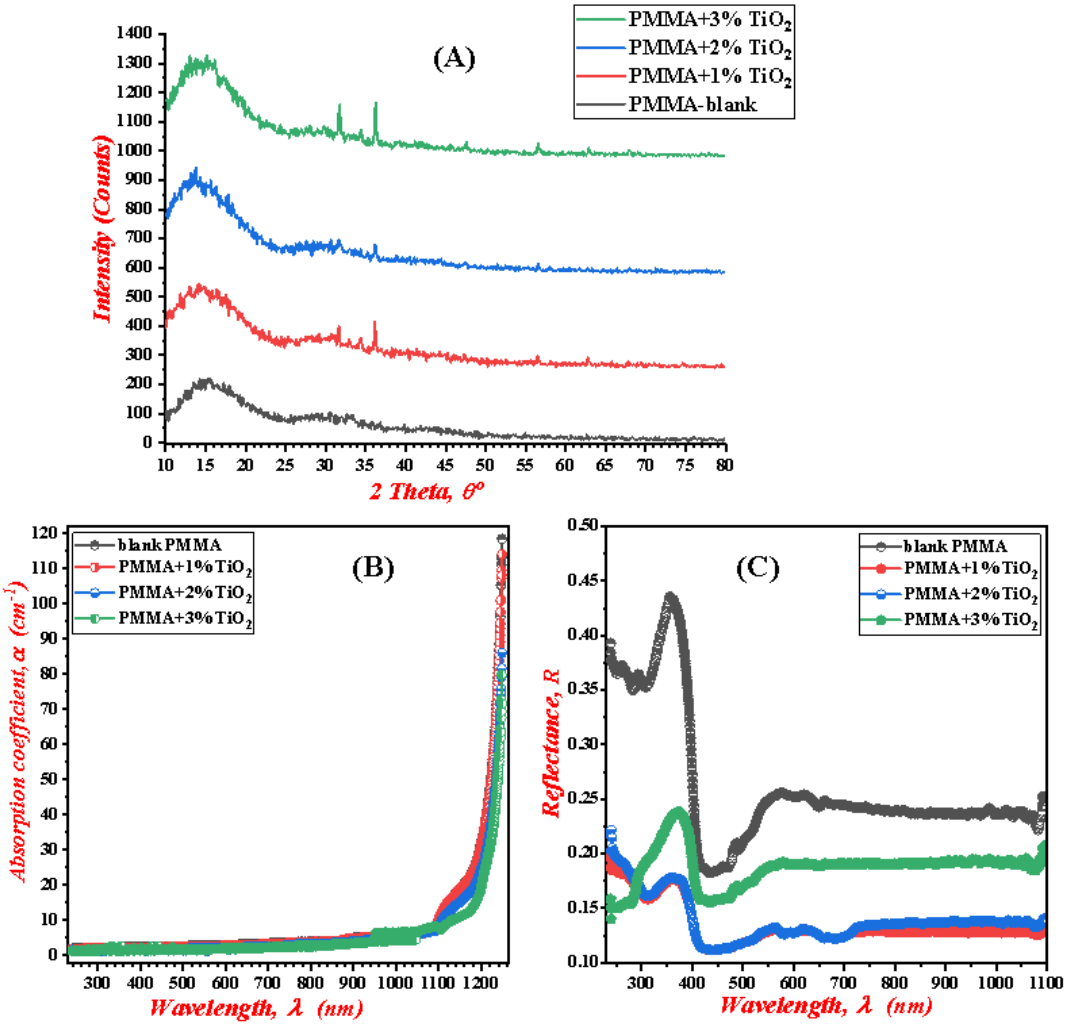

Figure 3. (A) XRD diffraction of PMMA/TiO_2 nanocomposite pattern, (B) absorption coefficient, (C) reflectance.

[40]:

$$n = \left[\frac{1+R}{1-R}\right] + \sqrt{\frac{4R}{(1-R)^2} - k^2} \tag{5}$$

where: (R) is reflectance and (k) is extinction factor. The refractive index of the blank PMMA and PMMA/TiO_2 nanocomposites shown in Fig. 4 (A).

Extinction factor (k) is related to the wavelength attenuation inside films, the attenuation denotes how far waves transfer within the thickness of the coating and refers to the loss of absorbance of the thin film. The extinction factor (k) is computed from the equation (6) [41]:

$$k = \frac{\alpha\lambda}{4\pi} \tag{6}$$

where: (α) is the absorption coefficient in (cm^{-1}) and (λ) is the wavelength in (nm), the extinction factor (k) of the blank PMMA and PMMA/TiO_2 nanocomposites films is shown in Fig. 4 (B).

Fig. 4 (A) shows that the refractive index reached 4.8 units after exposing the samples of nanocomposite films doped with TiO_2 to DBD plasma, where the polymer chain underwent structure change.

Also, Fig. 4 (B) shows the lower values of the extinction factor, where, these values are comparatively tinny and in the part from ten thousand region representing a minimum loss of absorption. where the process of undergone for the PMMA structure is done to the additive of TiO_2 nanoparticles and the exposure to DBD plasma [42].

3.4 Real and imaginary dielectric constant of PMMA/TiO_2

Real (ε_1) and imaginary (ε_2) dielectric constant (ε) is a distinguish to the energy storage, where the two parameters are very important to the electronic nature of the material. The two parameters depend on the refractive index (n) and extinction factor (k) and are computed from equation (7) [43]:

$$\left[[(\varepsilon) = \varepsilon_1(\omega) + i\varepsilon_2(\omega)]\right] \quad \varepsilon_1 = n^2 - k^2 \quad \varepsilon_2 = 2nk \tag{7}$$

So, the symbols of are: real (ε_1) and imaginary (ε_2).

The imaginary dielectric constant referred to the losses in absorption through the film for the blank PMMA and PMMA/TiO_2 nanocomposites, as shown in Fig. 4 (C).

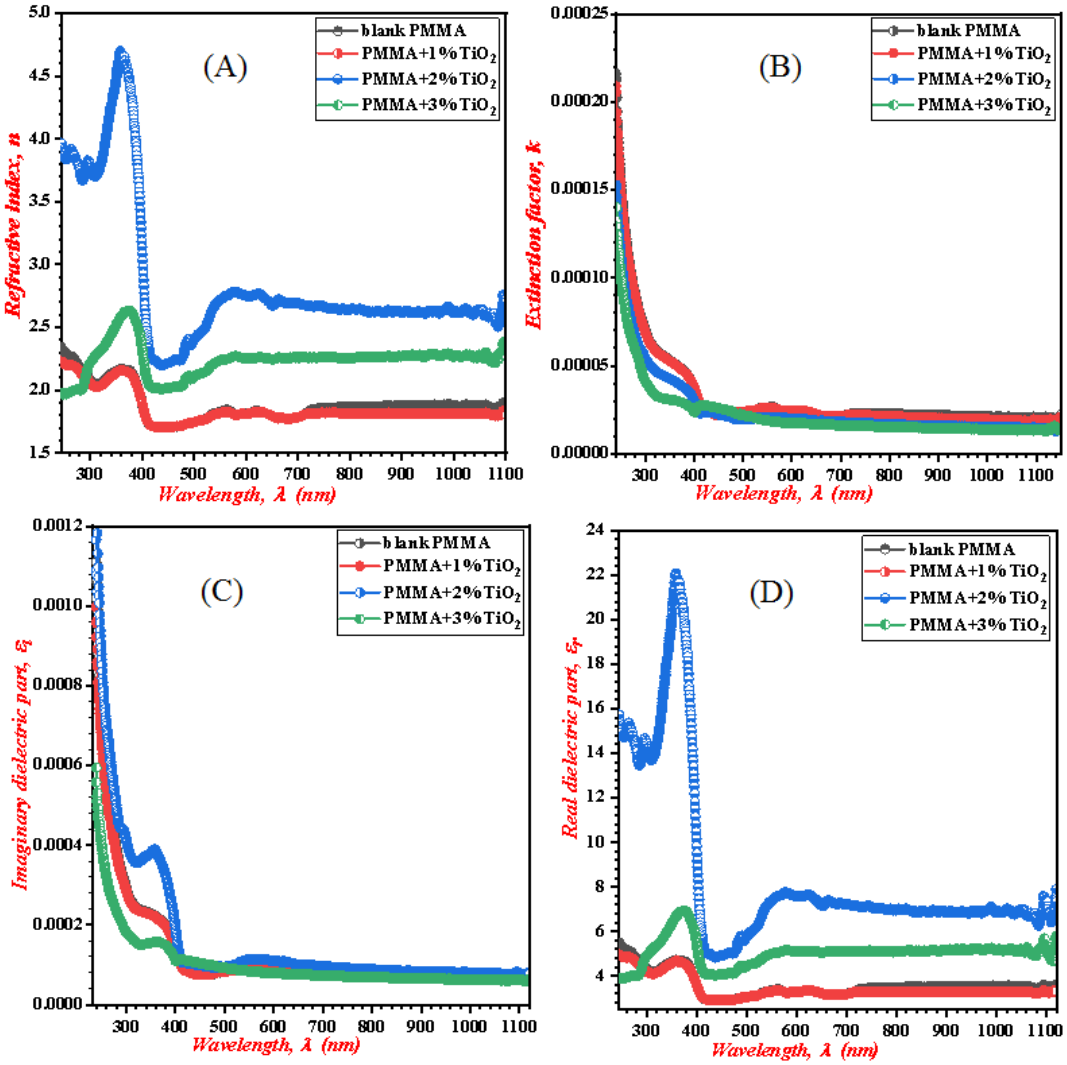

Figure 4. (A) Refractive index, (B) Extinction factor, (C) Imaginary dielectric part (D) Real dielectric part.

The real dielectric mentioned the storage of the light that is absorbed inside the film layer, therefore, Fig. 4 (D) shows the blank PMMA and PMMA/TiO_2 nanocomposites.

Fig. 4 (C) clearly shows that the values of the imaginary dielectric are relatively small and represent a fraction of thousands. These minuscule amounts of imagined components demonstrate that the films of the PMMA/TiO_2 nanocomposites and blank PMMA exhibit high absorbance and negligible absorbance losses. The changes in polymer chains are due to the addition of nanoparticles and their exposure to DBD plasma rays, which have given these results high values in absorption.

In a similar approach, the real dielectric constant displayed relatively high values, going up to 22 units in the visible region and then declaiming at a wavelength of about $\lambda > 600$ nm. Apart from this region, the change in the real dielectric constant continued as the wavelength increased along the x-axis. This boost might be associated with the doping of nanoparticles and the DBD plasma exposure, which affected the characteristics of the PMMA films, as shown in Fig. 4 (D) [44].

3.5 Direct and indirect energy gap of PMMA/TiO_2

The energy gap (E_g) is regarded as an essential parameter for electronic and optoelectronic systems. It is considered a major factor through which the material can be conductive or not. When the material is conductive the absorption will be very high. Hence, the energy gap (E_g) is computed from Tauc's relation (8) [45]:

$$(\alpha h\nu)^b = G(h\nu - E_g) \tag{8}$$

where: (G) a constant connected to the semiconductor structure, and (b) exponent denotes the type of allowed transition ($n = 2$ and 0.5 for direct and indirect transition) [46].

The $(\alpha h\nu)^n$ in contradiction of photon energy ($h\nu$) for the PMMA films is drawn in Fig. 5 (A) and 5 (B), the E_g is computed by captivating through the extrapolation to interrupt the E_{ph} line till the y-axis $(\alpha h\nu)^n$ equals zero. Fig. 5 (A) shows the direct transition and Fig. 5 (B) shows the indirect transition for the blank PMMA and PMMA/TiO_2 nanocomposites.

It can be clear from Fig. 5 (A) that the direct E_g ranges between 4.5 to 4.7 eV and can very closely between them for the blank PMMA and PMMA/TiO_2 nanocomposites, this

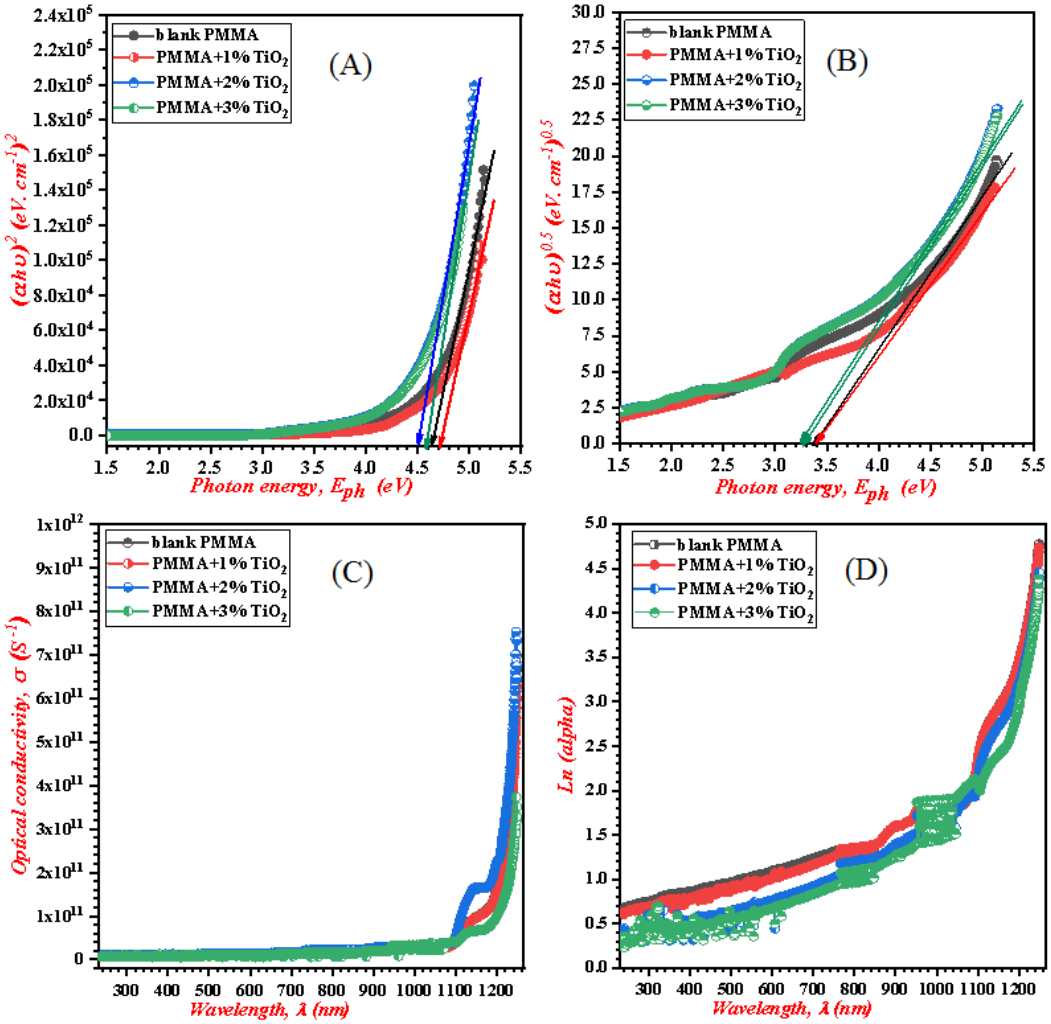

Figure 5. (A) Direct energy gap transition, (B) Indirect energy gap transition, (C) Optical conductivity, and (D) Urbach energy.

concurrence of values might be regarded to the modifications in the polymer chains after doping with nanoparticles and DBD plasma exposure. It's clear that the DBD plasma has a fundamental role in reorganizing particles inside the PMMA nanocomposite films, and as a result, the curves appeared in an enhanced and refined manner.

Also, it can be inferred from Fig. 5 (B) that the indirect E_g ranges between 3.3 to 3.4 eV and can be seen very close to each other for the films of PMMA nanocomposite, where this convergence of the values belong to change polymer chains after the addition of nanoparticles and the exposure the films to DBD plasma ray that given these results, where the DBD plasma work to arrange the particles of the PMMA nanocomposite films to appear these curves in the finest case [47].

3.6 Optical conductivity and Urbach energy of PMMA/TiO_2

Optical conductivity (σ_{opt}) signifies the conductivity created by a charge carrier that is jumping between the bands (valence and conduction), the charge carrier creates an electric field effect of polarization to the dipole associated with photons absorption through the wavelength light rays, permitting the motion for transference. The optical conductivity can be calculated from equation (9) [48]:

$$\sigma = \frac{\alpha n c}{4\pi} \tag{9}$$

Henceforth, (σ_{opt}) (S^{-1}), (c) light speed (3×10^{10} cm/s), (α) absorbance coefficient (cm^{-1}), and (n) refractive index. The disorders onto the energy gap and the tail unit of absorption are denoted by Urbach energy (E_u), which is considered the exponential increase of absorption with photon energy. It is related the localized states due to the existence of disorders in the material presented of additives the TiO_2 nanoparticles. Urbach energy replicates the intensity of absorbance for the nanocomposite film, it can be calculated from equation (10) [48]:

$$\alpha = \alpha_0 \exp \frac{h\nu}{E_u} \tag{10}$$

At this point, (α_0) constant, (E_u) Urbach energy (eV), and ($h\nu$) photon energy (eV).

Consequently, the logarithm of both sides is taken to equation (10) for rearrangement of the equation:

$$\ln \alpha = \ln \alpha_0 \frac{h\nu}{E_u} \tag{11}$$

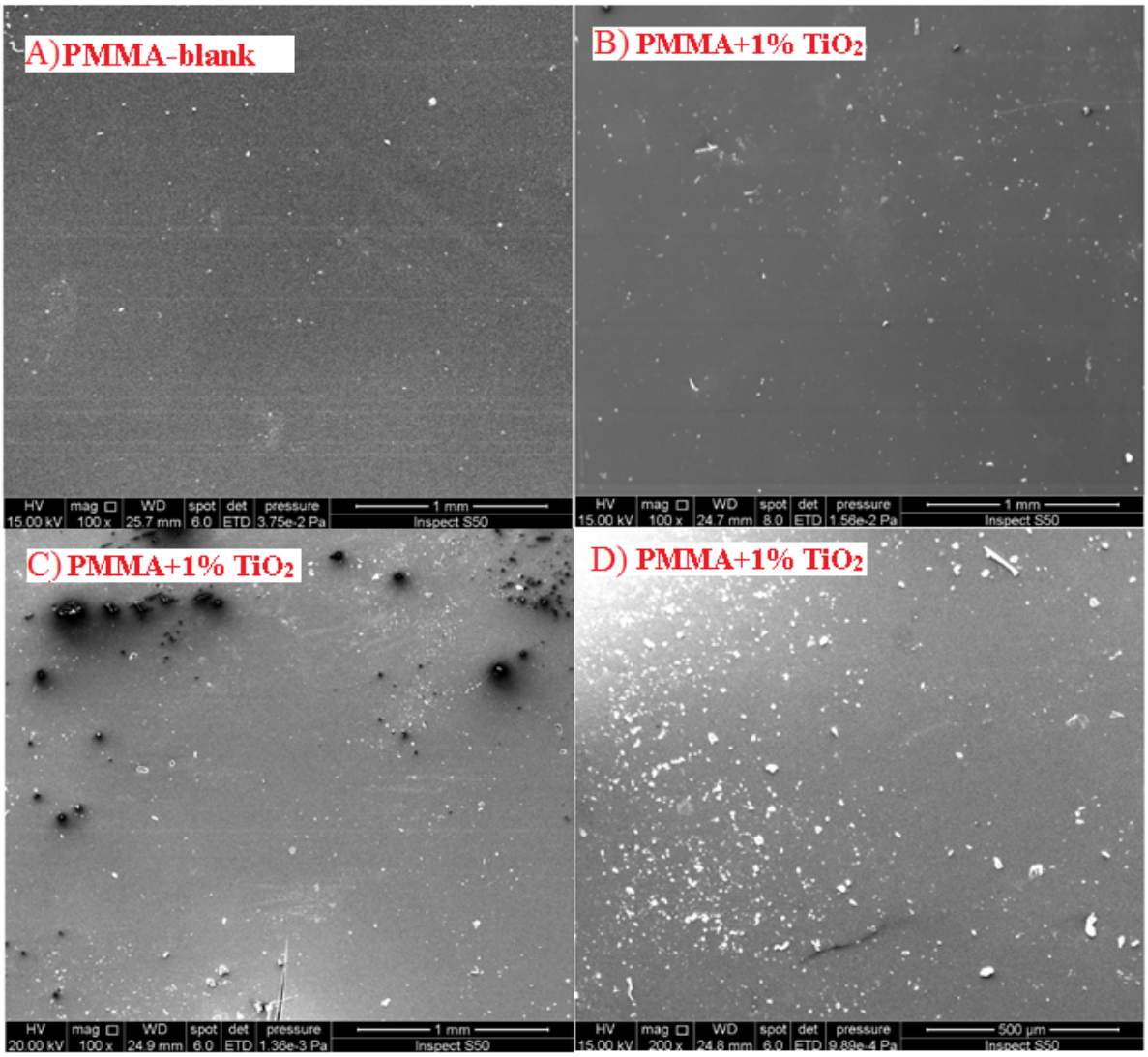

Figure 6. SEM images for the: (a) blank PMMA, (b) PMMA + 1% TiO_2, (c) PMMA + 2% TiO_2, and (d) PMMA + 3% TiO_2.

Therefore, the optical conductivity in Fig. 5 (C) and Urbach energy in Fig. 5 (D) for the blank PMMA and PMMA/TiO_2 nanocomposites with various filling concentrations of TiO_2. It can be inferred from Fig. 5 (C) that the optical conductivity increased after adding TiO_2 nanoparticles and being exposed to the DBD plasma, reaching values of 7.4×10^{11}. It is observed that exposing the PMMA nanocomposite structure to the plasma rays organizes the structure with nanoparticles to produce these results with high absorption. Also, Urbach energy as seen in Fig. 5 (D) has an increased value from 366 meV to 395 meV, where the structure of PMMA after adding TiO_2 nanoparticles is arranged to be optimum after exposed to DBD plasma rays [49].

Table 1 shows the direct energy gap, indirect energy gap, and urbach energy values for the blank PMMA and PMMA/TiO_2 nanocomposites after the addition of TiO_2 nanoparticles and exposure to DBD plasma rays.

4. SEM image of PMMA nanocomposite films

The examination of SEM is implemented to illustrate the surface morphology of incorporating TiO_2 in the PMMA matrix films as described in Fig. 6. Therefore, Fig. 6 (A) shows the blank PMMA is smooth and deprived of any nanoparticles of TiO_2 with small particles representing a white dot because it didn't blend during the mixing. Fig. 6 (B) shows a smooth surface and many white dots inside the PMMA matrix, these white dots denote 1% of TiO_2 addition, and the roughness of the surface is increased after exposure to the DBD plasma rays. Then, Fig. 6 (C) shows many white dots with many black patches, the white dots belong to the 2% of TiO_2 nanoparticles, and the black patches belong to the effect of DBD plasma rays and the roughness of the surface samples increased. Despite this fact, the miscibility of PMMA with increasing TiO_2 nanoparticles is accompanied by the occurrence leading to a non-smooth surface because of the penetration of TiO_2 nanoparticles into the PMMA film sheet. Thereby, Fig. 6 (D) shows a large number of white dots on the surface of PMMA belonging to the increasing number of nanoparticles of TiO_2, and its percentage is estimated at 3% after the addition, in this sample there is excellent miscibility of PMMA with TiO_2 and give most advantageous among the experimented samples, the surface is much rough than other samples due to the nanoparticles and exposing to DBD plasma rays [50–54].

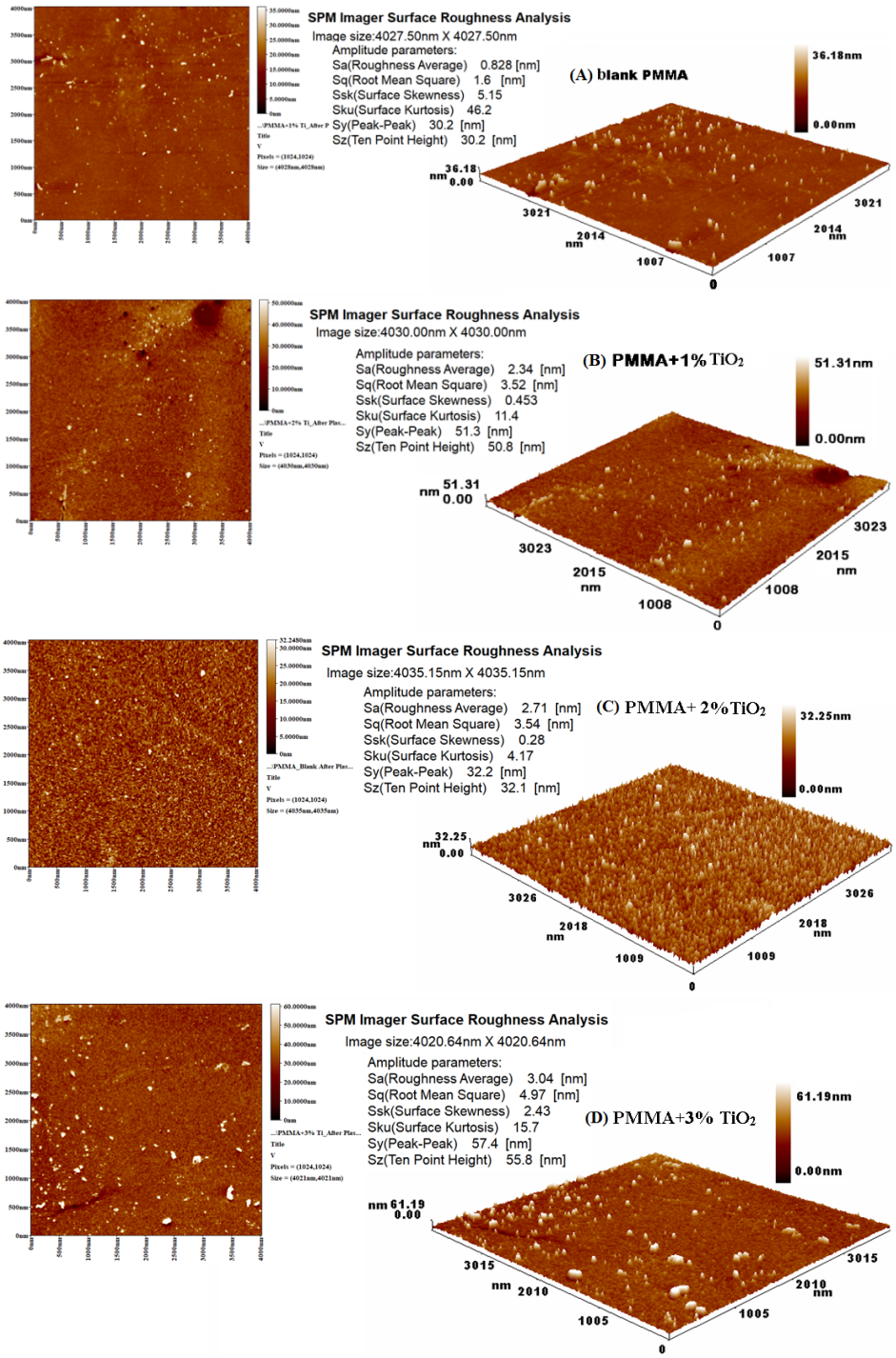

Figure 7. AFM images for the: (a) blank-PMMA, (b) PMMA + 1% TiO_2, (c) PMMA + 2% TiO_2, and (d) PMMA + 3% TiO_2.

5. AFM pictures of PVC films

The AFM analysis reveals insights into surface morphology through its 2D and 3D images, providing an understanding of both regular and irregular surface roughness characteristics that are sensitive to incident light. Numerous studies have emphasized the effectiveness of AFM in examining such surface features, as illustrated in Fig. 7. Subsequently, the surface roughness values are presented in the Supplementary Table **??**.

Fig. 7 presents AFM images of blank and nanocomposite films made from PMMA and TiO_2, aiming to evaluate the surface roughness of PMMA/TiO_2 nanocomposite films. It can be observed from Fig. 7 that the surface roughness and root mean square (RMS) values of particles are as follows: for blank PMMA as exhibited in Fig. 7 (A), 0.828 nm and 1.6 nm, for PMMA with a rate of 1% TiO_2 exhibited in Fig. 7 (B), 2.34 nm and 3.52 nm, for PMMA with a rate of 2% TiO_2 as exhibited in Fig. 7 (C), 2.71 nm and 3.54 nm, and for PMMA with a rate of 3% TiO_2 as exhibited in Fig. 7 (D), 3.04 nm and 4.91 nm, respectively. Table 1 inferences the surface roughness and RMS values of particles for pure and doping PMMA [55–58].

Table 1. Direct energy gap, indirect energy gap, and Urbach energy values.

No.	Parameters	PMMA blank	PMMA + 1% TiO_2	PMMA + 2% TiO_2	PMMA + 3% TiO_2
1	Direct transition of (E_g) (eV)	4.7	4.65	4.5	4.55
2	Indirect transition of (E_g) (eV)	3.4	3.4	3.25	3.3
3	Urbach energy (E_u) meV	366	380	366	395
4	(α_0) absorption constant (cm^{-1})	1.402	1.573	2.136	2.168

6. Conclusion

This work is designed to develop innovative nanostructured composite films based on poly(methyl methacrylate) (PMMA). Employing a casting method, these films were incorporated with titanium oxide (TiO_2) at different concentrations (1%, 2%, and 3%). The doping process is followed by exposure to an indoor assembled cold dielectric barrier discharge (DBD) plasma device. This instrument was essential to modify the structural and optical properties of the prepared nanocomposite films. The architectural rearrangement of nanoparticles induced by plasma treatment contributed to the enhancement of material properties.

Main optical parameters have thoroughly been computed directly from equations with their analysis, such as absorption coefficient, extinction factor, refractive index, energy gap, dielectric constant (real and imaginary), and Urbach energy. Results showed an increase in the absorption coefficient, refractive index, and real dielectric constant, on the other hand, the imaginary dielectric constant and the extinction coefficient decreased in values because of the improved light absorption. energy gaps (indirect and direct) were narrowed in space, going from 3.4 to 3.25 eV, and 4.7 to 4.5 eV, respectively. Urbach energy increases from 366 to 395 meV, showing an enhancement in the dynamics of charge carriers, which might be attributed to plasma-induced structural improvements.

Additionally, exposure to plasma was instrumental in enhancing surface roughness and crystallinity in the prepared nanocomposite films. XRD analysis verified the existence of both amorphous and semi-crystalline structures, with enhanced crystalline structures after incorporating TiO_2 and treatment with plasma. SEM imaging showed a rough-surfaces incorporated with better-organized nanoparticles inside the PMMA composite. AFM analysis confirmed a remarkable escalation in the roughness of the surface (SR) (blank 0.828 and PMMA/TiO_2 nanocomposite at 3.04 nm) and escalation in root mean square (RMS) (blank 1.6 and PMMA/TiO_2 nanocomposite at 4.97 nm) after TiO_2 doping.

These results emphasize the capability of the PMMA/TiO_2 prepared nanocomposite films for different progressive applications, such as developing optical sensors, chemical photocatalysis, manufacturing fibre optics, and light-emitting diodes (LEDs). Exposure to cold DBD plasma has been confirmed to effectively enhance the optical and structural properties of the polymer-based nanocomposites, laying a foundation for their applications in optoelectronic devices and environmental processes.

Acknowledgment

The Department of Mechanical Engineering in the College of Engineering and the Department of Chemistry in the College of Science at Al-Nahrain University provided access to laboratory facilities in order to partially assist the current effort.

Supplementary data

The supplementary data can be found in the file submitted with the manuscript.

Authors Contribution

Authors have contributed equally in preparing and writing the manuscript.

Availability of data and materials

The data that support the findings of this study are available from the corresponding author, upon reasonable request.

Conflict of interests

The authors declare that they have no known competing financial interests or personal relationships that could have appeared to influence the work reported in this paper.

References

[1] A.D. Mani, P.M.K. Reddy, M. Srinivaas, P. Ghosal, N. Xanthopoulos, and C. Subrahmanyam. Facile Synthesis of Efficient Visible Active C-Doped TiO_2 Nanomaterials with High Surface Area for the Simultaneous Removal of Phenol and Cr(VI). . *Mater. Res. Bull.*, **61**: 391–399, (2015).
DOI: https://doi.org/10.1016/j.materresbull.2014.10.051.

[2] T.J. Entradas, J.F. Cabrita, B. Barrocas, M.R. Nunes, A.J. Silvestre, and O.C. Monteiro. Synthesis of Titanate Nanofibers Co-Sensitized with ZnS and Bi_2S_3 Nanocrystallites and Their Application on Pollutants Removal. *Mater. Res. Bull.*, **72**:0–28, (2025).
DOI: https://doi.org/10.1016/j.materresbull.2015.07.008.

[3] C. Karunakaran, G. Abiramasundari, P. Gomathisankar, G. Manikandan, and V. Anandi. Preparation and Characterization of ZnO–TiO_2 Nanocomposite for Photocatalytic Disinfection of Bacteria and Detoxification of Cyanide under Visible Light. *Mater. Res. Bull.*, **46**: 1586–1592, (2011).
DOI: https://doi.org/10.1016/j.materresbull.2011.06.019.

[4] G. Cacciato, M. Bayle, A. Pugliara, C. Bonafos, M. Zimbone, V. Privitera, M.G. Grimaldi, and R. Carles. Enhancing Carrier Generation in TiO_2 by a Synergistic Effect between Plasmon Resonance in Ag Nanoparticles and Optical Interference. . *Nanoscale*, **7**:13468–13476, (2015).
DOI: https://doi.org/10.1039/C5NR02406D.

[5] A. Nicosia, F. Vento, G.M. Di Mari, L. D'Urso, and P.G. Mineo. TiO_2-Based Nanocomposites Thin Film Having Boosted Photocatalytic Activity for Xenobiotics Water Pollution Remediation. . *Nanomaterials*, **11**(400):1–11, (2021).
DOI: https://doi.org/10.3390/nano11020400.

[6] P. Wang, J. Wang, H. Yu, L. Zhao, and J. Yu. Hierarchically Macro-Mesoporous TiO_2 Film via Self-Assembled Strategy for Enhanced Efficiency of Dye-Sensitized Solar Cells. . *Mater. Res. Bull.*, **74**: 380–386, (2016).
DOI: https://doi.org/10.1016/j.materresbull.2015.11.004.

[7] Y. Shengyuan, Z. Peining, A.S. Nair, and S. Ramakrishna. Rice Grain-Shaped TiO_2 Mesostructures-Synthesis, Characterization, and Applications in Dye-Sensitized Solar Cells and Photocatalysis. *J. Mater. Chem.*, **21**:6541–6548, (2011).
DOI: https://doi.org/10.1039/C0JM04512H.

[8] A. Qu, X. Xu, H. Xie, Y. Zhang, Y. Li, and J. Wang. Effects of Calcining Temperature on Photocatalysis of G-C_3N_4/TiO_2 Composites for Hydrogen Evolution from Water. . *Mater Res Bull*, **80**:167–176, (2016).
DOI: https://doi.org/10.1016/j.materresbull.2016.03.043.

[9] V. Etacheri, C. Di Valentin, J. Schneider, D. Bahnemann, and S.C. Pillai. Visible-Light Activation of TiO_2 Photocatalysts: Advances in Theory and Experiments. . *J Photochem Photobiol C Photochem Rev*, **25**:1–29, (2015).
DOI: https://doi.org/10.1016/j.jphotochemrev.2015.08.003.

[10] S. Weon and W. Choi. TiO_2 Nanotubes with Open Channels as Deactivation-Resistant Photocatalyst for the Degradation of Volatile Organic Compounds. *Environ Sci Technol*, **50**:2556–2563, (2016).
DOI: https://doi.org/10.1021/acs.est.5b05418.

[11] L. Gao, Y. Wang, Y. Yan, Q. Li, C. Hao, and T. Ma. Enhanced Photoactivities of TiO_2 Particles Induced by Bio-Inspired Micro-Nanoscale Substrate. . *J Colloid Interface Sci*, **470**:10–13, (2016).
DOI: https://doi.org/10.1016/j.jcis.2016.02.029.

[12] A. Arabzadeh and A. Salimi. One Dimensional CdS Nanowire@TiO_2 Nanoparticles Core-Shell as High-Performance Photocatalyst for Fast Degradation of Dye Pollutants under Visible and Sunlight Irradiation. *J Colloid Interface Sci*, **479**:43–54, (2016).
DOI: https://doi.org/10.1016/j.jcis.2016.06.036.

[13] J. Zhang, L. Li, Z. Xiao, D. Liu, S. Wang, J. Zhang, Y. Hao, and W. Zhang. Hollow Sphere TiO_2–ZrO_2 Prepared by Self-Assembly with Polystyrene Colloidal Template for Both Photocatalytic Degradation and H_2 Evolution from Water Splitting. . *ACS Sustain Chem Eng*, **4**:2037–2046, (2016).
DOI: https://doi.org/10.1021/acssuschemeng.5b01359.

[14] M. Enculescu, A. Costas, A. Evanghelidis, and I. Enculescu. Fabrication of ZnO and TiO_2 Nanotubes via Flexible Electro-Spun Nanofibers for Photocatalytic Applications. *Nanomaterials*, **11**:1305, (2021).
DOI: https://doi.org/10.3390/nano11051305.

[15] A. Md Alamgir, G.C. Mallick, S.K. Nayak, and S. Tiwari. Development of PMMA/TiO_2 nanocomposites as excellent dental materials. *JMST*, **33**:4755–4760, (2019).
DOI: https://doi.org/10.1007/s12206-019-0916-7.

[16] V.K. Thakur and M.R. Kessler. Self-healing polymer nanocomposite materials: A review.". *Polym*, **69**:369–383, (2015).
DOI: https://doi.org/10.1016/j.polymer.2015.04.086.

[17] C.K. Sheng, K.A.M. Amin, L.L. Hong, M.F. Hassan, and M. Ismail. Investigation of Morphological, Structural and Electrical Properties of Cds/PMMA Nanocomposite Film Prepared by Solution Casting Method. *Int J Electrochem Sci*, **12**:10023–10031, (2017).
DOI: https://doi.org/10.20964/2017.11.75.

[18] J. Jordan, K.I. Jacob, R. Tannenbaum, M.A. Sharaf, and I. Jasiuk. Experimental Trends in Polymer Nanocomposites-A Review. . *Mater Sci Eng A*, **393**:1–11, (2005).
DOI: https://doi.org/10.1016/j.msea.2004.09.044.

[19] N.N. Hafizah, M.H. Mamat, C.M.S. Said, M.H. Abidin, and M. Rusop. Thermal Degradation of Nanocomposited PMMA/TiO_2 Nanocomposites. *IOP Conf Ser: Mater Sci Eng*, **46**:1–8, (2013).
DOI: https://doi.org/10.1088/1757-899X/46/1/012045.

[20] A.S. Hassanien and I. Sharma. Band-gap engineering, conduction and valence band positions of thermally evaporated amorphous Ge_{15-x} Sb_x Se_{50} Te_{35} thin films: Influences of Sb upon some optical characterizations and physical parameters. *J Alloys Compd*, **79**: 750–763, (2019).
DOI: https://doi.org/10.1016/j.jallcom.2019.05.252.

[21] U. Ali, K.J.B.A. Karim, and N.A. Buang. A Review of the Properties and Applications of Poly (Methyl Methacrylate) (PMMA). . *Polym Rev.*, **55**:678–705, (2015).
DOI: https://doi.org/10.1080/15583724.2015.1031377.

[22] N. Pandey, R. Khaling, P. Verma, P. Pendke, and A. Patel. Characterization of TiO_2 Doped Poly (Methyl Methacrylate) PMMA Thin Films Using XRD. *AIP Conf Proc.*, **2100**:020151, (2019).
DOI: https://doi.org/10.1063/1.5098705.

[23] S. Ghosh, A.K. Mallik, and R.N. Basu. Enhanced Photocatalytic Activity and Photoresponse of Poly(3,4-Ethylenedioxythiophene) Nanofibers Decorated with Gold Nanoparticle under Visible Light. *Sol Energy*, **159**:548–560, (2018).
DOI: https://doi.org/10.1016/j.solener.2017.11.036.

[24] A.M. Abdullah, L.H. Alwan, A.A. Ahmed, and R.N. Abed. Optical properties of polystyrene with carbon nanotube and carbon nano incorporated and surface morphology studies. *Int Nano Lett.*, **13**: 165–176, (2023).
DOI: https://doi.org/10.1007/s40089-023-00398-0.

[25] F. Rezaei, B. Shokri, and M. Sharifian. Atmospheric-pressure DBD plasma-assisted surface modification of poly methyl methacrylate: A study on cell growth/proliferation and antibacterial properties. . *Appl Surf Sci.*, **164**:471–481, (2015).
DOI: https://doi.org/10.1016/j.apsusc.2015.11.036.

[26] S.K. Taha, S.N. Mazhir, and M.K. Khalaf. A Comparative Study on the Electrical Characteristics of Generating Plasma by Using Different Target Sources. *Baghdad Sci J.*, **15**:436–440, (2018).
DOI: https://doi.org/10.21123/bsj.2018.15.4.0436.

[27] F. Wieland, R. Bruch, M. Bergmann, S. Partel, G.A. Urban, and D.C. Can. Enhanced Protein Immobilization on Polymers-A Plasma Surface Activation Study. *Polymers MDPI*, **12**:104, (2020).
DOI: https://doi.org/10.3390/polym12010104.

[28] U. Ali, G. Nagpal, I. Sharma, and S.K. Tripathi. The effect of substitution of Sb with Zn on the optical and physical properties of Se90Sb10-xZnx (x = 0, 2, 4, 6, 10 at. %) thin films. . *Optik*, **207**: 164460, (2020).
DOI: https://doi.org/10.1016/j.ijleo.2020.164460.

[29] S.M. Mahdi and M.A. Habeeb. Tailoring the structural and optical features of (PEO–PVA)/($SrTiO_3$–CoO) polymeric nanocomposites for optical and biological applications. . *Polym Bull*, **80**: 12741–12760, (2023).
DOI: https://doi.org/10.1007/s00289-023-04676-x.

[30] R.N. Abed, M.A. Sattar, S.S. Hameed, et al. Optical and morphological properties of poly(vinyl chloride)-nano-chitosan composites doped with TiO_2 and Cr_2O_3 nanoparticles and their potential for solar energy applications. . *Chem Pap.*, **77**:757–769, (2023).
DOI: https://doi.org/10.1007/s11696-022-02512-6.

[31] K.A. Aadim. Spectroscopic study the plasma parameters for SnO_2 doped ZnO prepared by pulse Nd:YAG laser deposition. . *IJP*, **17**: 125–135, (2019).
DOI: https://doi.org/10.30723/ijp.v17i42.447.

[32] H. Akatsuka. Optical Emission Spectroscopic (OES) Analysis for Diagnostics of Electron Density and Temperature in Non-Equilibrium Argon Plasma Based on Collisional-Radiative Model. . *Adv. Phys.:X*, **4**:1592707, (2019).
DOI: https://doi.org/10.1080/23746149.2019.1592707.

[33] Z.S. Jaber, M.A. Habeeb, and W.H. Radi. Synthesis and Characterization of (PVA-CoO-ZrO_2) Nanostructures for Nano optoelectronic Fields. *EEJP*, **2**:228–233, (2023).
DOI: https://doi.org/10.26565/2312-4334-2023-2-25.

[34] K.A. Ibrahim and K.A. Aadim. Spectroscopic Diagnosis of Cobalt Plasma Produced by OES Technique and Influence of Applied Voltage on Plasma Parameters. . *IJS*, **64**:2271–2281, (2023).
DOI: https://doi.org/10.24996/ijs.2023.64.5.15.

[35] A.A. Mohammed and M.A. Habeeb. Effect of Si_3N_4/TaC nanomaterials on the structural and electrical characteristics of poly methyl methacrylate for electrical and electronics applications. *EEJP*, **2**: 157–164, (2023).
DOI: https://doi.org/10.26565/2312-4334-2023-2-15.

[36] R.N. Abed, A.A. Rashad, M.H. Rahman, A. Basem, A. Al-Ani, A. Husain, N.S. Jumaah, H. Hashim, M.S. Bufaroosha, E. Yousif, and A. Hadawey. Synthesis, Structural, and Optical Properties of Modified Poly(vinyl Chloride) Thin Films by Ethylenediamine Loaded with Metal Oxide Nanoparticles. ". *ChemistrySelect*, **9**:1–17, (2024).
DOI: https://doi.org/10.1002/slct.202401717.

[37] A.M. Abdullah, L.H. Alwan, A.A. Ahmed, and R.N. Abed. Optical and Physical Properties for the Nanocomposite Poly(vinyl chloride) with Affected of Carbon Nanotube and Nano Carbon. *PCCC*, **16**: 331–345, (2023).
DOI: https://doi.org/10.30509/PCCC.2023.167082.1198.

[38] A.J.K. Algidsawi, A. Hashim, A. Hadi, and M.A. Habeeb. Exploring the characteristics of SnO_2 nanoparticles doped organic blend for low cost nanoelectronics applications. . *SPQEO*, **24**:472–477, (2021).
DOI: https://doi.org/10.15407/spqeo24.03.472.

[39] R.N. Abed, K. Zainulabdeen, M. Abdallh, E. Yousif, and A.A. Rashad. The optical properties behavior of modified poly(methyl methacrylate) nanocomposite thin films during solar energy absorption. . *J Non-Cryst Solids*, **609**:122257, (2023).
DOI: https://doi.org/10.1016/j.jnoncrysol.2023.122257.

[40] A.M. Abdullah, L.H. Alwan, A.A. Ahmed, and R.N. Abed. Physical Study of PVA Filled with Carbon Nanotube and Nano Carbon with Roughness Morphology. *J Phys Chem Res*, **11**:747–760, (2023).
DOI: https://doi.org/10.22036/PCR.2022.362088.2195.

[41] R.N. Abed, N.K. Al-Sahib, and A.J.N. Khalifa. Energy Gap Demeanor for Carbon Doped with Chrome Nanoparticle to Increase Solar Energy Absorption. . *PCCC*, **13**:143–154, (2020).
DOI: https://doi.org/10.30509/PCCC.2020.81613.

[42] H. Hashim, M. Ali, R.T. Abdulla, R.N. Abed, A. Basem, A.A. Rashad, M. Al-Baidhani, K.A. Aadim, A.H. Shaker, M.S. Bufaroosha, and E. Yousif. Influence of cold plasma treatment on the PS/TiO_2 film's optical properties of nanocomposite surfaces. . *Mater Lett*, **373**:137077, (2024).
DOI: https://doi.org/10.1016/j.matlet.2024.137077.

[43] R.N. Abed, M.H. Al-Mashhadani, E. Yousif, et al. Organosilane-doped PVC lattice thin film for optoelectronic applications. *J Opt.*, **53**:2247–2261, (2024).
DOI: https://doi.org/10.1007/s12596-023-01351-2.

[44] A.S. Hassanien and A.A. Akl. Effect of Se addition on optical and electrical properties of chalcogenide CdSSe thin films. . *Superlattice Microst.*, **89**:153–169, (2016).
DOI: https://doi.org/10.1016/j.spmi.2015.10.044.

[45] R.N. Abed, E. Yousif, A.R.N. Abed, and A.A. Rashad. Synthesis Thin Films of Poly(Vinyl Chloride) Doped by Aromatic Organosilicon to Absorb the Incident Light. . *Silicon*, **14**:11829–11845, (2022).
DOI: https://doi.org/10.1007/s12633-022-01893-3.

[46] Z.M. Al-Azzawi, M. Al-Baidhani, A.R.N. Abed, and R.N. Abed. Influence of Nano Silicon Carbide (SiC) Embedded in Poly(Vinyl Alcohol) (PVA) Lattice on the Optical Properties. . *Silicon*, **14**: 5719–5732, (2022).
DOI: https://doi.org/10.1007/s12633-021-01325-8.

[47] R.N. Abed, A.R.N. Abed, and E. Yousif. Carbon Surfaces Doped with (Co_3O_4-Cr_2O_3) Nanocomposite for High-Temperature Photo Thermal Solar Energy Conversion Via Spectrally Selective Surfaces. *PCCC*, **14**:301–315, (2020).
DOI: https://doi.org/10.30509/PCCC.2021.166749.1098.

[48] R.M. Omer, E.T.B. Al-Tikrity, R.N. Abed, M. Kadhom, A.H. Jawad, and E. Yousif. Electrical conductivity and surface morphology of PVB films doped with different nanoparticles. . *PCCC*, **15**:191–202, (2022).
DOI: https://doi.org/10.30509/PCCC.2021.166839.1120.

[49] A. Ahmed, R.N. Abed, M. Kadhom, H. Hashim, E. Akram, A. Jawad, and E. Yousif. Modification of poly (vinyl chloride) thin films with organic compound and nanoparticles for solar energy applications. . *J Polym Res*, **30**:03654–1, (2023).
DOI: https://doi.org/10.1007/s10965-023-03654-1.

[50] K. Zainulabdeen, R.N. Abed, and E. Yousif. Optical systematic and morphological characterization of PMMA thin films containing copper(II) and zinc(II) chloride additives for selective surfaces. *Phys Chem Res*, **12**:1091–1110, (2024).
DOI: https://doi.org/10.22036/pcr.2024.477090.257.

[51] A. Hashim, A.J. Kadham, A. Hadi, and M.A. Habeeb. Determination of Optical Parameters of Polymer Blend/Nanoceramics for Electronics Applications . *Nanosist. Nanomat. Nanotehnol*, **19**:327–336, (2021).
DOI: https://doi.org/10.15407/nnn.19.02.327.

[52] R.S.A. Hamza and M.A. Habeeb. Reinforcement of morphological, structural, optical, and antibacterial characteristics of PVA/CMC bioblend filled with SiO_2/Cr_2O_3 hybrid nanoparticles for optical nanodevices and food packing industries. *Polym. Bull.*, **81**:4427–4448, (2024).
DOI: https://doi.org/10.1007/s00289-023-04913-3.

[53] I. Oreibi, M. Ali Habeeb, and R.S. Abdul Hamza. Polymer nanocomposites comprising PVA matrix and Ag–$BaTiO_3$ nanofillers: a comparative study of structural, dielectric and optical characteristics for optics and quantum nanoelectronic applications. *Opt. Quant. Electron.*, **56**:05685, (2024).
DOI: https://doi.org/10.1007/s11082-023-05685-w.

[54] A.M. Salam, M.Y. Rahimi, A. Mohammed, A. Rasheed, S.A. Dina, A.A. Ahmed, A.A. Ahmed, A. Basheer, and Y. Emad. Additives Aid Switch to Protect the Photodegradation of Plastics in Outdoor Construction. . *NJES*, **22**:277–282, (2019).
DOI: https://doi.org/10.29194/NJES.22040277.

[55] D. Zageer, W. Al-Taa'y, H. Ibraheem, A. Hasan, and E. Yousif. Optical Properties and Morphological Study of New Films Derived From Poly(Vinyl Chloride)-Phenyl Phrine HCl Acid Complexes. . *ANJS*, **19**:51–57, (2016).
DOI: https://doi.org/10.22401/JNUS.19.2.07.

[56] P. Emir and D. Kuru. Boron nitride quantum dots/polyvinyl butyral nanocomposite films for the enhanced photoluminescence and UV shielding properties. . *J. Appl. Poly. Sci.*, **141**:55171, (2024).
DOI: https://doi.org/10.1002/app.55171.

[57] M.A. Habeeb and S.M. Mahdi. Influence of ZrC nanofiler on the structural, dielectric and optical features of the PVA–PVP blend for electronic and optical nanodevices. *Opt. Quant. Electron.*, **55**:05426, (2023).
DOI: https://doi.org/10.1007/s11082-023-05426-z.

[58] M. Essam, A. Elsayed, A. Nasser, et al. Processing of Ti–5Al–4W–2Fe Alloy Using Different Powder Metallurgy Routes to Improve Its Implementation in Structural Applications. . *Arab J Sci Eng*, (2025).
DOI: https://doi.org/10.1007/s13369-024-09834-5.

Supplementary figure 1. (a): XRD device utilized to inspect the structure of the nanocomposite films PMMA/TiO_2, the diffraction angle (2θ) ranged from 10° to 80° to exhibit the film's structure crystalline or amorphous. (b) Diffusive reflectance utilized to inspect the PMMA/TiO_2 films.

Supplementary figure 2. AFM (AA2000) to illustrate the surface roughness of PMMA/TiO_2 thin films.

Supplementary Table 1. The compositions of the samples for blank PMMA and PMMA/TiO_2 nanocomposite thin films.

No.	Sample	TiO_2 (% wt.)	PMMA (g)
1	blank PMM	0	1.5
2	PMMA + 1% TiO_2	1	1.5
3	PMMA + 2% TiO_2	2	1.5
4	PMMA + 3% TiO_2	3	1.5

Supplementary Table 2. DBD plasma parameters result for AC applied voltage of (10) kV.

High Voltage (kV) (kV)	T_e (eV)	$\Delta\lambda_{FWHM}$ (nm)	$n_e \times 10^{18}$ (cm^{-3})	$f_p \times 10^{13}$ (Hz)	$\lambda_D \times 10^{-5}$ (cm)
10	1.624	6.89	5.0291	20.138	21.240

Supplementary Table 3. Roughness values of PMMA/TiO_2 nanocomposite films.

No.	Composite	Figure's number	Roughness average (SR) (nm)	Root mean square (RMS) (nm)
1	PMMA blank	7-a	0.828	1.6
2	PMMA + 1% TiO_2	7-b	2.34	3.52
3	PMMA + 2% TiO_2	7-c	2.71	3.54
4	PMMA + 3% TiO_2	7-d	3.04	4.97

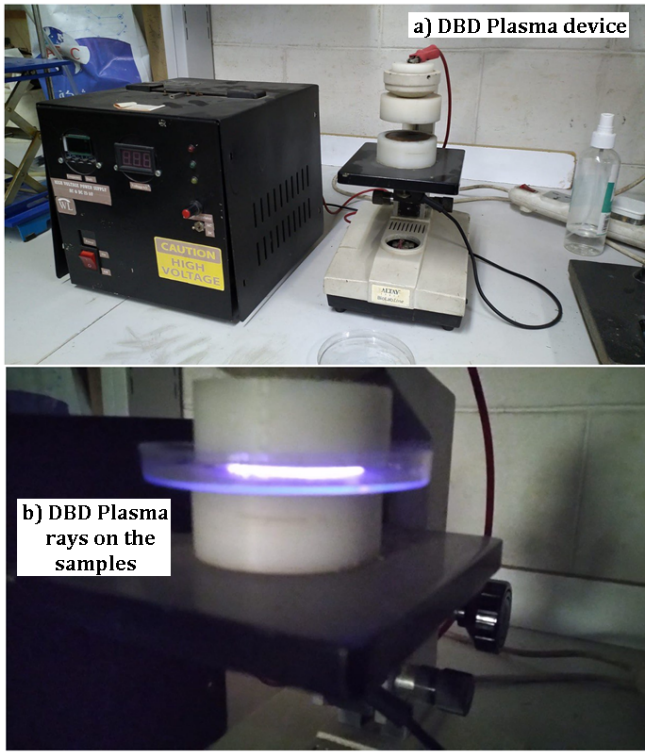

Supplementary figure 3. (a and b): Cold plasma DBD device utilized to strike the sample by a plasma ray in its chamber.